Eur Biophys J (2003) 32: 392–401
DOI 10.1007/s00249-003-0284-0

ARTICLE

Georgios Papadopoulos · Thomas Hauß

# Determination of the number of water molecules in the proton pathway of bacteriorhodopsin using neutron diffraction data

Received: 24 September 2002 / Accepted: 2 January 2003 / Published online: 12 March 2003


**Abstract** It has been shown that water molecules participate in the proton pathway of bacteriorhodopsin. Large efforts have been made to determine with various biophysical methods the number of water molecules involved. Neutron diffraction $H_2O/D_2O$ exchange experiments have been often used to reveal the position of water even with low-resolution diffraction data. With this technique, care must be taken with the limitations of the difference Fourier method which are commonly applied to analyze the data. In this paper we compare the results of the difference Fourier method applied to measured diffraction data (not presented here) and models with those from alternative methods introduced here: (1) a computer model calculation procedure to determine a label's scattering length density based on a comparison of intensity differences derived from models and intensity differences from our measurements; (2) a method based on the Parseval formula. Both alternative methods have been evaluated and tested using results of neutron diffraction experiments on purple membranes (Hauss et al. 1994). Our findings indicate that the difference Fourier method applied to low-resolution diffraction data can successfully determine the position of localized water molecules but underestimates their integrated scattering length density in the presence of labels in other positions. Furthermore, we present the results of neutron diffraction experiments on purple membranes performed to determine the number of water molecules in the projected area of the Schiff base at 86%, 75% and 57% relative humidity (r.h.). We found $19 \pm 2$ exchangeable protons at 75% r.h., which means at least 8–9 water molecules are indispensable for normal pump function.

**Keywords** Bacteriorhodopsin · Neutron diffraction · Proton pathway · Purple membranes · Water molecules

**Abbreviations** BR: bacteriorhodopsin · CC: correlation coefficient · DF: difference Fourier · EL: extended label · LL: local label · PM: purple membrane · r.h.: relative humidity

G. Papadopoulos (✉)
Department of Biochemistry and Biotechnology,
University of Thessaly, Ploutonos 26,
41221 Larisa, Greece
E-mail: papg@chem.auth.gr

T. Hauß
BENSC/SF2, Hahn-Meitner-Institut Berlin,
14109 Berlin, Germany

T. Hauß
Institut für physikalische Biologie,
Heinrich-Heine-Universität Düsseldorf,
Universitätsstrasse 1, 40225 Düsseldorf, Germany

## Introduction

Early neutron diffraction experiments on purple membranes (PMs) in 100% relative humidity (r.h.) (Zaccai and Gilmore 1979) showed that the area of highest H/D exchange is the lipid region. The difference Fourier maps could not reveal a water channel spanning the membrane in the protein region. Our previous neutron diffraction studies (Papadopoulos et al. 1990) on PMs at very low hydration (15% r.h. or less) showed the existence of about 3–4 (according to the difference Fourier method) tightly bound water molecules in the projected region of the Schiff base (i.e. the proton pathway of bacteriorhodopsin, BR)[1]. At higher hydration, more water molecules at the same position were expected (Dencher et al. 1992). To see if, at higher hydration (closer to physiological conditions), a larger number of water molecules is present in the transmembrane proton pathway, we performed neutron diffraction experiments at 57%, 75% and 86% r.h. (Hauß et al. 1997) correlated to the results of time-resolved laser spectroscopy (Thiedemann et al. 1992). The analysis of the data of these experiments with our usual data treatment was not

[1]The light absorbing system of bacteriorhodopsin is the "retinal" connected to Lysin216 of the protein's backbone via a protonated Schiff base in the ground state

able to reveal more water molecules than those we found at very dry PMs. Even worse, at 75% and 86% r.h. we found fewer water molecules than at 57% r.h. This was an unexpected and paradoxical result. In order to resolve this, we examined all steps in our data evaluation process using model calculations (presented in this paper) and we have found the following main sources of error:

1. Low-resolution data.
2. Use of both ratios for overlapping reflections (see Materials and methods) and phases from electron microscopy with neutron scattering data.
3. The presence of an extended scattering length density distribution in the difference map beside that localized at the region of the Schiff base.

Recently, high-resolution X-ray and electron microscopy structures of wild-type and mutated BR (Belrhali et al. 1999; Luecke et al. 1999; Sass et al. 2000; Subramaniam and Henderson 2000) have been published. The X-ray studies show about nine functional water molecules participating in the proton pathway in the ground state. The M state (one of the intermediates of the BR photocycle) shows about three water molecules more. These structures represent a fully hydrated state of BR grown in the lipid cubic phase. The question is: "How many water molecules in the proton conducting pathway of BR are really essential for normal function?" To answer this question, we have to determine the number of water molecules at the critical hydration levels for the pump function at 75% and 86% r.h. (Thiedemann et al. 1992). In order to overcome the limitations of the difference Fourier (DF) method, we introduce here two alternative methods and we evaluate the data of our previous experiments according to them.

In the following sections we first present in Materials and methods our neutron diffraction experiments and then the usual data treatment. In following sections we describe the model calculations to analyze the different error contributions. Then we present a computer model calculation procedure referred here as "simulation". This method scans NatMod [the neutron scattering length density distribution of an atomic model of the PM constructed by Edholm et al. (1995) projected onto a 128×128 two-dimensional matrix; it is used here as a model starting structure] with a circular label of defined radius and scattering length distribution. Secondary labels and extended labels are also probed. The calculated intensity differences between every resulting map and the original map are then compared to experimental intensity differences. This procedure is very reliable in finding the position of local labels (LLs)[2]. It is also better than the DF method in determining the total scattering length of local labels at higher hydration. No presumptions (beside the use of a model for a BR trimer) about phases and ratios of overlapping reflections are needed. We provide a detailed description of the procedure in Appendix 1. In the next section we present another method to calculate the integrated scattering length density of an LL based on the Parseval formula. This method is valid only for single-label difference maps and is described in detail in Appendix 2. Finally, in the Results and discussion section we present the results of the above methods.

[2]What we call here a local label is a label with a narrow distribution of its total scattering length compared to the experimental resolution; a file of water molecules almost perpendicular to the membrane plane behaves like a local label

## Materials and methods

### Neutron diffraction

PMs were isolated and prepared as described elsewhere (Papadopoulos et al. 1990). The diffraction sample is a stack of lamellar oriented PMs (100 mg), which gives rise to powder reflections (many of them are overlapping) due to in-plane rotational averaging in the membrane stack. During data collection the sample is kept in a thermostatted aluminum can where the humidity is adjusted with saturated salt solutions in $H_2O$ or $D_2O$, respectively ($H_2O/D_2O$ exchange). The samples were equilibrated for a couple of days before data collection. Diffraction experiments were carried out on the Membrane Diffractometer V1 at the Berlin Neutron Scattering Center of the Hahn-Meitner-Institut, Berlin, Germany. Diffraction patterns were measured in a $\theta$-$2\theta$ experimental setup at $\lambda = 5.686$ Å and $T = 25$ °C. Data reduction was done using the local instrument software. Owing to the relatively large divergence of the neutron primary beam, the shape of the diffraction peaks is essentially Gaussian. Fitting Gaussian functions to the experimental data and applying a Lorentz correction determined the diffraction intensities:

$$I_c = I\sqrt{h^2 + hk + k^2} \tag{1}$$

Structure factor amplitudes were derived taking the square root of the intensities.

### The usual method to determine the position and strength of a label from a difference map

For a two-dimensional lattice, the distribution of the label's scattering length density is given by the difference Fourier sum (Blundell and Johnson 1976):

$$\Delta\rho(x,y) = \frac{1}{A}\sum_{h\neq 0}\sum_{k\neq 0}\left(\left|F_{hk}^{\mathrm{nl}}\right| - \left|F_{hk}^{\mathrm{n}}\right|\right)\exp\left(i\phi_{hk}^{\mathrm{n}}\right)\exp(-2\pi i(hx+ky)) \tag{2}$$

where $|F^{\mathrm{nl}}|$ and $|F^{\mathrm{n}}|$ are the amplitudes of the structure factors of the labeled and native structure, respectively, $\phi^{\mathrm{n}}$ are the phases of the native structure and $A$ is the area of the elementary cell. The calculated $\Delta\rho$ is half as intense compared to the original (Blundell and Johnson 1976). In Appendix 4 we demonstrate that the previous statement is valid for high-resolution data, assuming correct phases for the native structure. In a powder diffraction pattern, intensities located at the same distance from the origin of the reciprocal space are overlapping. In order to obtain the structure factors $F_{hk}$ and lacking (in the past) a better choice, we had to use both phases and split ratios of overlapping reflections derived from electron microscopy (Henderson et al. 1986).

The scattering length distribution calculated from Eq. (2) represents only relative contrasts between different parts of the elementary cell. The final step is to sum up $\Delta\rho$ over an area that is expected to be covered by the label.

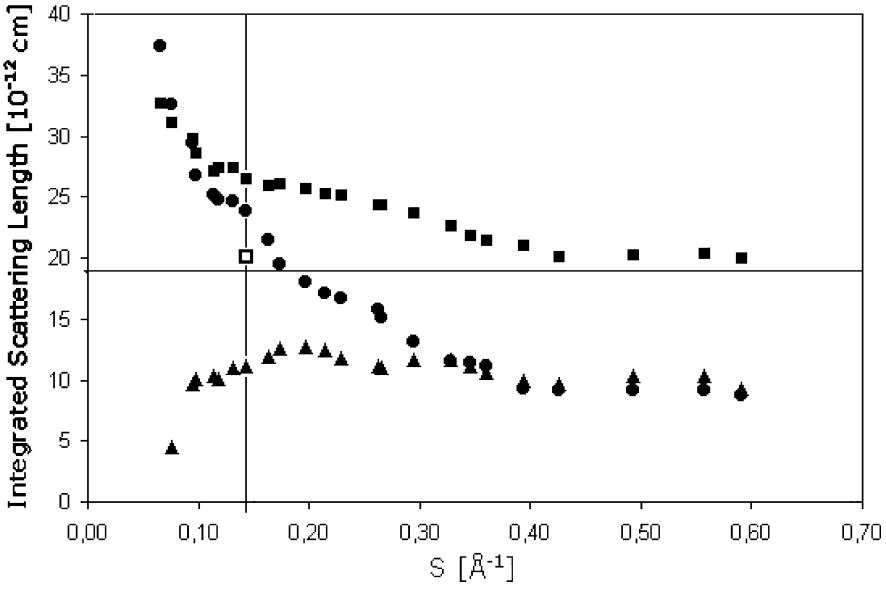


**Fig. 1** The effect of resolution on the integrated scattering length density of the reconstructed label after DF with only phases from NatMod (*filled squares*), with phases and split ratios from NatMod (*filled circles*), with phases and split ratios from NatMod + extended label (*filled triangles*), and with phases and split ratios from electron microscopy (*open squares*). The *vertical line* denotes our experimental resolution. The *horizontal line* denotes the value for the integrated scattering length density predicted by DF ($17.55\times10^{-12}$ cm) at high resolution

### Model calculations to test the limitations of the usual data analysis

In this paper we use as a starting structure an atomic model of the PM constructed by Edholm et al. (1995) by molecular dynamics calculations using electron microscopy data for BR derived from the literature. In this model, the missing loop amino acids and lipids (modeled as phosphatidylglycerol) were added prior to the MD calculations. After adding the missing protons to the PDB structure and assigning for every atom its neutron scattering length, we project this scattering length distribution onto a 128×128 two-dimensional matrix in order to derive a scattering length $X$-$Y$ density map. The best agreement between the calculated intensities and those from experiment has been obtained by omitting the carboxyl terminus. This is justified by the flexibility of the carboxyl terminus. The corresponding distribution is what we call here the "native model" (NatMod). This is clearly a better choice than using data from electron microscopy, because the correlation coefficient between our measured neutron scattering intensities and those calculated from NatMod (0.958) is larger than that between our data and those from electron microscopy (0.735).

Next we put the experimental intensities on the same scale as those calculated from the model, adjusting the sum of the Lorentz-corrected experimental intensities to that of the model. We separate their intensity contributions according to split ratios of NatMod. The amplitude of the structure factor is then simply the square root of the intensity. The phases $\phi^{n}$ of the native structure are those calculated from NatMod.

In order to resolve the extent of the different error contributions, a series of calculations is presented below, each time taking into account a different error source.

### PM contains one local label

The starting structure for our model calculation is NatMod. To simulate the neutron diffraction and data evaluation we proceed as follows:

1. Perform a numeric Fourier transform on NatMod to obtain a set of ($|F^{n}|,\phi^{n}$) with the desired resolution. NatMod simulates a dehydrated PM.
2. Now add to NatMod a label by covering an almost circular area of variable radius around the Schiff base nitrogen with the desired total scattering length. We call this structure the "labeled model" (LabMod), which simulates a locally hydrated PM.
3. As in step 1, LabMod is Fourier transformed to obtain a set of ($|F^{nl}|,\phi^{nl}$).
4. We apply then Eq. (2) (difference Fourier) using the data set ($|F^{nl}|-|F^{n}|,\phi^{n}$) to determine the label.

The label is a distribution of a neutron scattering length of $11.7\times10^{-12}$ cm, corresponding to six water molecules covering an almost circular area of 45 matrix points per monomer or 8.8 Å$^2$. The dimensions have been chosen in a way so that the label can be regarded as a LL for our experimental resolution ($h=7$, $k=1$) $\rightarrow S=0.1429$ Å$^{-1}$ or 7 Å.

To study the effect of the central assumption of the DF method (phases from the NatMod), we have reconstructed the label at a different resolution (from $S=0.085$ Å$^{-1}$ to $S=0.59$ Å$^{-1}$). We then summed up after reconstructing the scattering length distribution over the position of the label for every resolution. In order to integrate the scattering length distribution we had to define the area of integration at each resolution level and to adjust the zero level of the difference density map. For this purpose, we developed the numerical algorithms described in Appendix 3.

### PM contains two labels, a local label and an extended label

A homogeneous neutron scattering length distribution ($202.67\times10^{-12}$ cm/trimer) over an area of about that of the lipids (referred to as an extended label, EL)[3] has been added to LabMod to simulate the surface $D_2O$ hydration. It corresponds to 106 $D_2O$ molecules distributed over 5065 matrix points per trimer. We now repeat the procedure of the previous section. The result of varying the resolution is shown in Fig. 1 (triangles).

### Simulation procedure to determine labels from low-resolution neutron diffraction data of PMs

The procedure relies on the comparison of the difference in radial intensities from a PM sample measured both in $H_2O$ and $D_2O$ atmospheres with the calculated difference in radial intensities from a model. The model is step-by-step modified, aiming at an improvement of the similarity between the data sets. As similarity

[3] A label with its scattering length distributed over a much wider area compared to the experimental resolution; hydration water that covers lipid areas of the elementary cell behaves like an extended label; both kinds of labels are present in the case of hydrated PMs

parameters we used the correlation coefficient (CC), the *R*-factor and $\chi^2$, which are defined in Appendix 1. In Appendix 1 we also present a detailed description of the simulation method. This is a tedious and a less direct procedure than the difference Fourier method, but it has the advantage of avoiding any serious assumptions about phases and split ratios for the overlapping reflections.

### Determining the strength of a local label by applying the Parseval formula

In the case of only one LL with a defined area in the difference map, there is an additional method to determine its total scattering length. This method relies on the Parseval formula and is described in Appendix 2. Since for this we need only the intensities, we avoid strong assumptions about phases and we do not need to define an integration area for the label. Both of the above introduce errors inherent in the case of the DF method. However, since we need $(\Delta|F|)^2$, prior to calculating $\Delta|F|$ we have again to split overlapping intensities according to NatMod. A further approximation is that we assume a homogeneous distribution of the label over its area.

Equation (19) (see Appendix 2) can be applied to determine the number of exchangeable protons in the proton pathway of BR. As already mentioned, this method can be applied if only one label of defined area is present in the difference map. Therefore we use it to determine the number of exchangeable protons at a very low hydration (15% r.h.) and the number of water molecules removed after extreme drying.

## Results and discussion

In the present study we look for water molecules that participate in the proton conduction pathway across BR. Such water molecules must be accessible by bulk protons under normal pump function conditions. The pump function is dramatically disturbed at r.h. conditions lower than 75%. Since we measure H/D exchange, we have to take into account that the exchange kinetics become slower by dehydration. This can result in a lower number of experimentally determined water molecules at very low r.h. On the other hand, at very high r.h. levels we expect that some water molecules are too "labile" to be determined by diffraction methods. So we have chosen the conditions 86%, 75% and 57% r.h. as the best compromise. We can attribute the paradoxical previous finding of a higher D/H exchange in the proton pathway at 57% r.h. compared to that at 75% either (1) to the sample preparation or (2) to the applied data evaluation. We exclude counting errors or other experimental conditions as the source of this paradox.

1. Since the swelling and spectroscopic behavior of the sample has been tested, we can exclude the biological sample as the source of the errors. At high r.h. the equilibration period is long enough to let most of the water molecules be exchanged in the proton pathway. At very low r.h., $H_2O/D_2O$ exchange may be incomplete during the equilibration period (60 h at room temperature). Since only exchanged water molecules will contribute to the difference map, this can lead to an underestimation of the number of water molecules for this r.h. Of course, this cannot explain the effect that we did not see more water molecules in the proton pathway at high hydration than at a medium one. The only factor that can lead to a reduced number of water molecules is the higher "mobility" of some water molecules at high r.h.
2. We consider effects arising from the data evaluation. The data treatment comprises Lorentz correction of measured intensities, absolute scaling and finally application of the difference Fourier method. The kind of Lorentz correction factor used can indeed affect the final result (i.e. the integrated scattering density of the label). In order to determine both the direction and the extent of this effect, we have tried different Lorentz factors on the data at 57% and 75% r.h. We multiplied $\Delta|F|$ values with the linear function $f(S) = 1 + 2S$, which enhances higher orders more than lower. The final result is 13% higher in both hydration levels. We repeated this calculation with $f(S) = 1-2S$, which suppresses higher orders more than lower. The final result is 13% lower in both hydration levels. Since we "correct" both data sets with the same function, we cannot expect that different monotonic functions can invert the results for 57% and 75% r.h. In our opinion the main errors in the result originate from the rest of the data treatment, namely application of both ratios for overlapping reflections and phases from electron microscopy with neutron scattering data. Furthermore, low resolution and the presence of an extended scattering length distribution as well as one in the region of the Schiff base nitrogen in the difference map, make the determination of the strength of a label difficult.

### Model calculations of the integrated scattering length density

The results of the model calculations described above (one LL) are shown in Fig. 1 (squares). Evidently the application of the DF method weakens the strength of the reconstructed label. Everywhere in this paper we do not multiply the reconstructed label by a factor of 2, as the DF method suggests. Furthermore, the DF method introduces a small artificial secondary peak "ghost" in the two-dimensional density map (not shown here). As expected, the value predicted by DF (half of the original) is reached at higher resolution. If we reconstruct the label using phases and split ratios for overlapping reflections from NatMod, we obtain the results shown in Fig. 1 (circles). At our experimental resolution (vertical line) the label's integrated scattering length density has been reconstructed 1.5 times weaker instead of twice as predicted by DF. Upon introducing ratios of the overlapping reflections and phases from electron microscopy, the integrated scattering length distribution is calculated for a resolution corresponding to our experiments (Fig. 1, open squares). The reconstructed scattering length distribution is 1.8 times weaker instead of twice as predicted by DF. At high resolution the integrated

scattering length density of the LL in the presence of an EL (model calculations described above) reaches the value of the former one when it stands alone (Fig. 1, triangles). At our experimental resolution the LL appears to be three times weaker than the original instead of twice as predicted by DF.

The absolute numbers presented above can vary, depending on the algorithm we use to sum up the integrated scattering length distribution of the label. Anyway, a suppression of a LL at low resolution in the presence of an EL is an obvious fact. This conclusion is critical in determining by DF the strength of the labels in two-dimensional difference density maps.

## Application of the DF method to our experimental data

In a normal DF map the only approximation made is the use of native phases for both the native and the labeled structures. The label emerges with half of its real total scattering length, given that we use high-resolution data. Our model calculations simulating a label at the Schiff base show that, at a resolution of $S = 0.118$ Å$^{-1}$, no correction by a recovering factor of 2 is needed. It is remarkable that, for a resolution of $S = 0.143$ Å$^{-1}$, if both phases and splitting ratios originate from electron microscopy, the label emerges with half of its real strength. Reevaluation of previous data (Papadopoulos et al. 1990) applying DF and corrections according to our model calculations (see above), we obtained $12 \pm 2$ D/H at 15% r.h. This is equivalent to $6 \pm 1$ water molecules. Application of the same procedure to our measurements at higher r.h. leads to $15 \pm 2$ D/H at 57% r.h. and $8 \pm 2$ D/H at 75% r.h. At 86% r.h. there is no clearly defined maximum at the projected area of the Schiff base. It is not satisfactory that even after the correction according to our model calculations the integration of the scattering length distribution in difference maps is unable to provide satisfactory results at hydration corresponding to higher than 57% r.h.

## Application of the simulation method to our experimental data

Application of the simulation method to our experimental data leads to $19 \pm 2$ D/H at 75% and $22 \pm 2$ D/H at 86% r.h. Unfortunately, the results for 57% r.h. are not reliable. This is because at this hydration neither the LL nor the EL applies very well. The model we used to simulate surface hydration has proved to be not realistic enough, especially leading to some difficulties in determining the extended labels at high r.h. data.

## Application of the Parseval formula to our experimental data

Application of the Parseval formula to D/H exchange data at 15% r.h. gave ~14 exchangeable protons per BR monomer. The same method applied to difference data between PM at 15% r.h. in $D_2O$ and after extreme drying gave ~6 removed water molecules per BR monomer.

## Combined results

We summarize the combined results of applying all the methods presented in this paper in Table 1. We accept for 15% r.h. the value 14 D/H provided from the Parseval formula, because this method is very reliable for very low r.h. At 57% r.h., we accept the result given by DF. For 75% and 86% r.h., we accept the results from the simulation method, 19 D/H and 22 D/H, respectively.

The results of the present work are in full agreement with the findings of the X-ray studies (Sass et al. 2000). At 75% r.h., where the M-decay time is ~10 times longer than at 86% r.h., we found $19 \pm 2$ exchangeable protons or $8 \pm 1$ water molecules. At this humidity level the pump retains its basic functionality and rehydration is still possible. It seems to be likely that at least 8 water molecules are necessary for pump function. At least 9 water molecules are needed to reach full functionality.

Beside the role of water as a proton-conducting medium, we would like to focus on another possible role for it related to the pump function (Ferrand et al. 1993). The most striking difference between the density maps at 86% and 75% concerns surface water removed mainly from the lipid areas of the PM. Dehydration of the lipid heads leads to less flexibility, limiting the range of the necessary conformational changes of BR. Furthermore, the interlamellar spacing of the PM stacks filled by water is also drastically shrunk upon dehydration. Since all steps of the photocycle (except the light driven *cis-trans* isomerization of the retinal) are relaxation processes depending on thermal energy, it is likely to relate the loss of water to a reduced thermal conduct of BR to the environment and a reduced rate of energy dissipation.

**Table 1** Number of exchangeable protons and water molecules present in or removed from the proton pathway of BR

| R.h. (%) | D/H exchanged ($\pm 2$) | WM present ($\pm 1$)[a] | WM removed ($\pm 1$)[b] |
|---|---|---|---|
| 86 | 22 | 9 | |
| | | | 1 |
| 75 | 19 | 8 | |
| | | | 1 |
| 57 | 16 | 7 | |
| | | | 1 |
| 15 | 14 | 6 | |
| | | | 6 |
| 0 | Not measured | – | |

[a]The number of water molecules that are compatible with the number of exchangeable protons at each relative humidity level, leaving 2–3 exchangeable protons in the proton pathway not belonging to the water molecules

[b]The number of water molecules that are compatible with the difference in exchangeable protons between two hydration levels

Considering the above, even if no water molecule of the proton pathway has been removed, the pump will slow down by reducing surface and interlamellar water.

**Acknowledgements** The authors are grateful to Professors G. Büldt and N. Dencher for helpful discussions.

## Appendix

### Appendix 1: the simulation method

The procedure to determine the position and scattering length density of a LL was evaluated using the known structure of BR (Edholm et al. 1995). The neutron scattering length density of a unit cell was projected onto the plane of the membrane to derive a model of the natural dry membrane (NatMod). At the in-plane position of the Schiff base the scattering length of 10 $H_2O$ or 10 $D_2O$ molecules was added on a circular area of $\sim$9 Å$^2$ per monomer. The additional scattering length simulated the presence of a file of 10 $H_2O$ or 10 $D_2O$ molecules perpendicular to the plane of PM. The structures created in this way simulated experimental samples equilibrated in a $D_2O$ or $H_2O$ atmosphere, respectively. Fourier transformation of these structures provided intensity pairs and their differences. These differences were then compared with intensity differences derived from trial structures, which were produced as described below. As similarity parameters between the sets of the intensity differences, we used the correlation coefficient, the $R$ factor and $\chi^2$. Systematic trials with up to three labels per monomer, equivalent to 10, 6 and 3 water molecules, at the same time gave the following results concerning the method.

The CC is a very effective criterion to determine the position of the label but less effective for the determination of its strength. The $R$ and $\chi^2$ are less sensitive in position and more sensitive in strength. The $R$ factor gave more reliable results than $\chi^2$ and therefore in the following only CC and $R$ are used as similarity parameters. If a label has strength comparable to the Fourier termination error, it is impossible to determine its position working in real space. For a resolution of 7 Å ($S=0.1429$) the termination error is about 10% of the strength of the strongest label. The localization of the two larger labels was sufficiently good. It was also possible to determine their strength. Unfortunately, this was not possible in the case of the weakest label.

The procedure for the case of both a LL and an EL together was evaluated using as a model for an EL a $H_2O$ or $D_2O$ monolayer defined by an area covering the lipid area of the PM elementary cell. This area was derived from density maps representing H/D exchange at high r.h. The LL was equivalent to 10 water molecules at ($x=18.4$, $y=0.5$) with a radius of 1.0 Å. All coordinates in this article are given in Å. These labels (both $D_2O$ and $H_2O$) were added to NatMod to simulate hydrated PM at high r.h. The Fourier transform of the derived structures provided a set of pairs of intensities for PM-$D_2O$ and PM-$H_2O$, respectively. Intensity differences were calculated without scaling of the data to each other. For the sake of the evaluation of the simulation method, these intensity differences represent the measured differences. During the simulation procedure we have tried to match them and the intensity differences from trial modifications of NatMod.

During trials we realized that it was more convenient to start the calculations with the determination of the EL and then proceed to determine the LL. The region of the EL was varied stepwise and for every step also the scattering length that we add on NatMod was varied. This was done, first in a coarse way by varying the level that determines the area in steps of 5% and then repeating in steps of 1% around the best area found. For every level the scattering length was varied until no further improvement of the similarity parameters was obtained.

After the determination of the EL followed the determination of the LL. This was done by adding the EL on NatMod and started the calculations as for LL. We repeated then the determination of the EL starting with NatMod modified by the LL previously found. The cyclic procedure was terminated when no further improvement of the comparison parameters was obtained.

In the case of the model, our simulation method revealed perfectly the location and the strength of the added labels. Also in the case of scaled intensities the results accurately represented the model, even if the converging was slower.

After successful evaluation of the method, we applied it to data from neutron diffraction experiments.

#### Coarse determination of the position of a label

The steps used were:

1. To determine a first estimate of the label position, a test label scanned the asymmetric part (one third) of the elementary cell in steps of 4 Å in both directions.
2. For every label position the CC and $R$-factor were calculated between experimental ($\Delta I_e$) and calculated intensity ($\Delta I_m$) differences. A candidate for the coarse label position is the one with the highest CC.

These steps were repeated with labels of different radius and strength. The position corresponding to the best CC and $R$ was chosen.

#### Fine determination of a label position

The above procedure was repeated by scanning the region around the position that had been defined by the coarse determination. The step width was 0.5 Å. The strength and radius of the test label was that defined at the end of the above section. The final position of the label was the one with the highest CC.

Determination of a label's strength and size

The first procedure was repeated, holding the test label at the position that had been defined by the second procedure and varying its strength and size. The best strength/radius combination was the one corresponding to the minimal $R$.

The above three steps defined accurately the position, the strength and the size of a localized area label. In the case where more than one LL was present, the described cyclic procedure determined the strongest of them. In order to determine a possible second label, we started the first procedure with the NatMod, modified by adding the first label. At the end of the above procedure the second label was determined.

To refine the strength and the position of the first label, the first procedure had to be started again with the NatMod modified by adding the previously determined second label. After fixing the parameters for the first label, the second one could be refined.

The cyclic procedure had to be terminated if the similarity parameters did not improve any more. Trials with scaled intensities showed no effect on the final result, but the procedure converged more slowly.

We tested the above simulation method by applying it to the scaled neutron diffraction data of BR, with specifically deuterated retinals (Hauss et al. 1994). In the sample called D11, eleven protons of the retinal have been exchanged with deuterons, while in the sample called D5, only five have been exchanged near the Schiff base linkage.

Using the proposed simulation method, the label D11 has been localized at ($x=20.3$, $y=12.1$), close to the position at ($x=20.8$, $y=12.6$) given by Hauss et al. (1994). The simulation method overestimated the number of deuterons to 12.3 with an error of +11%. The radius was found to be 1.5 Å.

In a next step the determination of the D11 label was tested by calculating CC and $R$ with the intensity differences weighted by $(1-\epsilon)$, where $\epsilon$ is the relative error in intensity. The result was again a position at ($x=20.3$, $y=12.1$), the number of deuterons 9.9 and the radius = 0.5 Å.

Finally, the method was tested by reducing the diffraction resolution, taking into account 25 ($S=0.1183$) intensities instead of the full set of 35 intensities ($S=0.1429$). No remarkable differences in the results were observed.

Considering D5, its position has been found at ($x=18.9$, $y=4.4$), with the scattering length corresponding to 7 deuterons and a radius of 4.4 Å. The simulation method overestimated both the strength and size of the label. The reason for this deviation is that D5 represents only 0.5% of the maximum contrast in the elementary cell.

Considering that the simulation method leads to very good results concerning the position and the strength of D11 and that 11 deuterons are equivalent to 5.5 $D_2O$ molecules, it is reasonable that the application of this method to our data for the $H_2O/D_2O$ exchange experiments at different r.h. will reveal the correct number of water molecules at the projected area of the Schiff base.

We used the following definitions for the similarity parameters:

$$\mathrm{CC}=\frac{N\sum(\Delta I_\mathrm{m}\Delta I_\mathrm{e})-\sum\Delta I_\mathrm{m}\sum\Delta I_\mathrm{e}}{\sqrt{N\sum(\Delta I_\mathrm{m})^2-(\sum\Delta I_\mathrm{m})^2}\sqrt{N\sum(\Delta I_\mathrm{e})^2-(\sum\Delta I_\mathrm{e})^2}} \tag{3}$$

$$R=100\frac{\sum||\Delta I_\mathrm{e}|-|\Delta I_\mathrm{m}||}{\sum|\Delta I_\mathrm{e}|} \tag{4}$$

$$\chi^2=\frac{\sum(\Delta I_\mathrm{m}-\Delta I_\mathrm{e})^2}{\Delta I_\mathrm{e}} \tag{5}$$

where $N$ is the number of intensities.

Appendix 2: calculation of the total scattering length of a label according to the Parseval formula

The scattering density distribution is reconstructed from the structure factors according to:

$$\rho(x)=\frac{1}{L}\sum_{h=-\infty}^{\infty}F(h)\exp(-2\pi ihx) \tag{6}$$

In the above equation, "$x$" and "$h$" stand for "$x,y$" and "$h,k$", respectively.

In the following we drop the factor $1/L$, since in the final formula we introduce a factor adapting numerical results to theory. Integrating $\rho(x)$ over $x$ we obtain:

$$\begin{aligned}\int_{-\infty}^{\infty}\rho(x)\,\mathrm{d}x&=\int_{-\infty}^{\infty}\sum_{h=-\infty}^{\infty}F(h)\exp(-2\pi ihx)\,\mathrm{d}x\\&=\sum_{h=-\infty}^{\infty}F(h)\int_{-\infty}^{\infty}\exp(-2\pi ihx)\,\mathrm{d}x\end{aligned} \tag{7}$$

According to a property of the delta function, the last integral of the above equation is $\delta(h)$. This means that the total scattering density over the entire elementary cell originates from $F(0)$, while $\sum_{h\neq0}F(h)\exp(-2\pi ihx)$ gives positive and negative contributions, which cancel out in the sum over the entire elementary cell. After this introduction it is obvious that we can rewrite $\rho$(x) as follows:

$$\begin{aligned}\rho(x)&=\rho_0+\rho_x\ \text{ with }\ \rho_0=F(0)\ \text{ and }\ \rho_x\\&=\sum_{h\neq0}F(h)\exp(-2\pi ihx)\end{aligned} \tag{8}$$

So at every one position "$x$" the scattering density $\rho(x)$ is $\rho_x$ (with the property $\sum_x\rho_x=0$) over a homogeneous background of $\rho_0$. For the numerical calculations we replace $\rho_x$ with $\rho_i$. The above considerations are valid also for the DF maps.

According to the Parseval formula (Killingbeck and Cole 1971), if $F(s)$ is the Fourier transform of $\rho(x)$, then:

$$\int_{-\infty}^{\infty} |\rho(x)|^2 \, \mathrm{d}x = \int_{-\infty}^{\infty} |F(s)|^2 \, \mathrm{d}s \text{ or numerically } \sum_{\mathrm{i}} (\rho_0 + \rho_i)^2 = \sum_j I_j \tag{9}$$

where $l_j = |Fj|^2$ and "$j$" indexes the reciprocal space.

From Eq. (9):

$$\sum_i \rho_i^2 + 2\rho_0 \sum_i \rho_i + \sum_i \rho_0^2 = \sum_j I_j \tag{10}$$

Because $\sum_i \rho_i = 0$, Eq. (10) gives:

$$\sum_i \rho_i^2 + \sum_i \rho_0^2 = \sum_{j \neq 0} I_j + I_0 \tag{11}$$

In our experiments:

$$I_0 = 0 \Rightarrow \rho_0 = 0 \Rightarrow \sum_i \rho_0^2 = 0 \tag{12}$$

Finally:

$$\sum_i \rho_i^2 = \sum_{j \neq 0} I_j \tag{13}$$

In a difference map, the only source of $\sum_i \rho_i^2$ is the label and $I_j = |\Delta F_j|^2$. So the sum provides the sum of the square of the local scattering length density over the area of the label. So far we have not used any phases at all but we still do not know $\Delta F$.

According to the cosine rule:

$$|\Delta F|^2 = |F^{\mathrm{nl}}|^2 + |F^{\mathrm{n}}|^2 - 2|F^{\mathrm{nl}}||F^{\mathrm{n}}| \cos(\phi^{\mathrm{nl}} - \phi^{\mathrm{n}}) \tag{14}$$

As is made clear from Fig. 2, $\cos(\phi^{\mathrm{nl}} - \phi^{\mathrm{n}}) \approx 1$, at least for labels similar to a file of 10 $D_2O$ molecules perpendicular to the membrane plane, so we can rewrite Eq. (14) as:

$$|\Delta F|^2 = \left(|F^{\mathrm{nl}}| - |F^{\mathrm{n}}|\right)^2 \text{ and } I = |\Delta F|^2 = \left(|F^{\mathrm{nl}}| - |F^{\mathrm{n}}|\right)^2 = (\Delta |F|)^2 \tag{15}$$

The method according to Parseval avoids the use of phases but it cannot avoid the more or less arbitrary splitting of the overlapping reflections to calculate $\Delta|F|$. The diffraction data at 15% r.h. (in $D_2O$ and $H_2O$ atmospheres) show significant intensity differences in eight reflections with Miller indices (1,0), (1,1), (1,2), (3,0), (4,0), (4,1), (1,4), (4,3). Four of them, (1,2), (4,1), (1,4), (4,3), are overlapping. Significant differences between data measured at 15% r.h. in $D_2O$ and data at 0% r.h. show 10 reflections: (1,0), (1,1), (2,0), (1,2), (3,0), (2,2), (4,0), (3,2), (4,1), (1,4). Four of them, (1,2), (3,2), (4,1), (1,4), are overlapping.

Since $\rho(x,y)$ is unknown, in order to apply Eq. (13) we must assume that the label is a homogeneous distribution of a mean scattering length density $d$ per matrix point over an area of a total of $n$ matrix points. This is justified for low resolution. So Eq. (13) is rewritten as:

$$nd^2 = \sum_{j \neq 0} I_j \tag{16}$$

If $n$ is known, then:

$$d = \sqrt{\frac{\sum_j I_j}{n}} \tag{17}$$

or the total scattering length of the label is:

$$D = nd = \sqrt{n \sum_j I_j} \tag{18}$$

Model calculations using a label each time spread on a different number of matrix points $n$ showed that if $\rho_i$ is the calculated scattering density of the label, then Eq. (13) holds for any resolution by introducing a constant proportionality factor before $\Sigma I_j$. This factor accounts for any constant coefficients needed for the correct application of the Fourier transform, which we omitted so far. The same calculations showed that for low resolution or for narrow distribution of the label the calculated $\sum_i \rho_i^2$ is much smaller than that from the

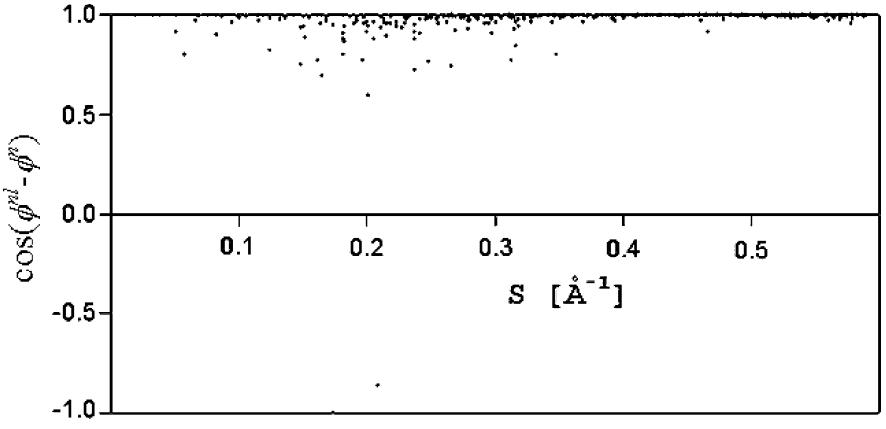


**Fig. 2** The value of $\cos(\varphi^{\mathrm{nl}} - \varphi^{\mathrm{n}})$ from Eq. (14) versus resolution for data from model calculations. The label is a circular distribution of scattering length density at the in-plane position of a Schiff base equivalent to 10 $D_2O$ molecules

model. In order to apply Eq. (18) to low-resolution data, we determined a correction dependent on $n$ as $\sim 1/n$. Considering the above, Eq. (18) takes the form:

$$D = nd = 9175\sqrt{\sum_j I_j} \tag{19}$$

In order to test Eq. (19), we applied it to experimental data of known total scattering length (Hauss et al. 1994). Sample D11 (known to have 11 protons/monomer replaced by deuterons at the retinal ring) gave 10.5 D/H or only 5% less. D5 (known to have 5 protons/monomer replaced by deuterons at the retinal end) gave 7.3 D/H or 45% more. This is a satisfactory result, given that D5 is a weak label. With the Parseval formula we were able to determine the D11 label with an accuracy of 5% and the weak D5 label with 45% accuracy.

Before applying Eq. (19), the data must have been scaled according to NatMod.

## Appendix 3: integration of a label's scattering length density

In order to sum up the scattering length density over the region of the label, we have firstly to define this region and secondly to adjust the zero level of the difference density map. The latter is necessary because of the absence of $\Delta F(0,0)$, which has the effect of suppressing the label by raising the zero level. In the presence of only one label (three in a threefold symmetry) it is possible to restore the zero level to its original height by demanding that the area of the density map outside the label must fulfill the condition $\sum_i \rho_i = 0$. So the first step is to define the area of the label. This is a somewhat complicated task, given that we deal with 2D maps and that the position as well as the area of the label can vary with the resolution and other parameters. We applied two methods to define the region of the label. According to the first, starting from the position of a maximum in the scattering length density we radially scan this region and define all matrix points as belonging to the label until we have found a minimum. According to the second method, matrix points around a maximum belong to the label if their scattering length density exceeds a predefined level compared to the total contrast in the elementary cell. The second step is to exclude the area of the label from the 128×128 matrix and calculate a suitable offset to ensure that $\sum_i \rho_i = 0$ in the non-label regions. In a third step we add this offset to the whole matrix and sum up over the already defined region of the label.

## Appendix 4: the peak heights in difference Fourier

A label is reconstructed by applying:

$$\Delta\rho(x,y) = \frac{1}{A}\sum_{h\neq 0}\sum_{k\neq 0} \left|F^{\mathrm{l}}_{hk}\right| \exp(i\phi^{\mathrm{l}}_{hk}) \exp(-2\pi i(hx+ky)) \tag{20}$$

In difference Fourier, $\left|F^{\mathrm{l}}_{hk}\right| \exp(i\phi^{\mathrm{l}}_{hk})$ is approximately replaced by $(\left|F^{\mathrm{nl}}_{hk}\right| - \left|F^{\mathrm{n}}_{hk}\right|) \exp(i\phi^{\mathrm{n}}_{hk})$:

$$\Delta\rho(x,y) = \frac{1}{A}\sum_{h\neq 0}\sum_{k\neq 0} (\left|F^{\mathrm{nl}}_{hk}\right| - \left|F^{\mathrm{n}}_{hk}\right|) \exp(i\phi^{\mathrm{n}}_{hk}) \times \exp(-2\pi i(hx+ky)) \tag{21}$$

The features of the DF map are determined by the following contributions (Blundell and Johnson 1976):

$$\begin{aligned}
&(\left|F^{\mathrm{nl}}_{hk}\right| - \left|F^{\mathrm{n}}_{hk}\right|) \exp(i\phi^{\mathrm{n}}_{hk}) \\
&= \frac{1}{\left|F^{\mathrm{nl}}_{hk}\right| + \left|F^{\mathrm{n}}_{hk}\right|} \left|F^{\mathrm{l}}_{hk}\right|^2 \exp(i\phi^{\mathrm{n}}_{hk}) \\
&+ \frac{1}{\left|F^{\mathrm{nl}}_{hk}\right| + \left|F^{\mathrm{n}}_{hk}\right|} \left|F^{\mathrm{n}}_{hk}\right| \left|F^{\mathrm{l}}_{hk}\right| \exp(i\phi^{\mathrm{l}}_{hk}) \\
&+ \frac{1}{\left|F^{\mathrm{nl}}_{hk}\right| + \left|F^{\mathrm{n}}_{hk}\right|} \left|F^{\mathrm{n}}_{hk}\right| \left|F^{\mathrm{l}}_{hk}\right| \exp(i(-\phi^{\mathrm{l}}_{hk} + 2\phi^{\mathrm{n}}_{hk}))
\end{aligned} \tag{22}$$

In our model calculations, $\left\langle \left|F^{\mathrm{l}}\right| \right\rangle \approx 0.1 \langle |F^{\mathrm{n}}| \rangle$ and $\left\langle \left|F^{\mathrm{nl}}\right| \right\rangle \approx \langle |F^{\mathrm{n}}| \rangle$, where the symbol $\langle\rangle$ denotes the average.

The first right-hand term of Eq. (22) is a weak reconstruction of the native structure of the order $0.05|F^{\mathrm{l}}|$. The second right-hand term of Eq. (22) contributes with half of $|F^{\mathrm{l}}|$. An inspection of the behavior of the factor $|F^{\mathrm{n}}|/(|F^{\mathrm{n}}| + |F^{\mathrm{nl}}|)$ versus $S$ (Fig. 3) shows that this factor

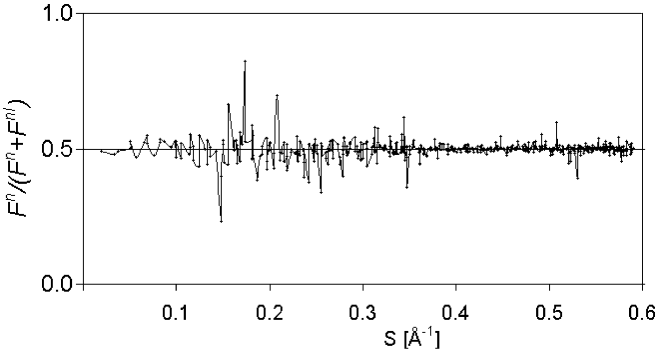


**Fig. 3** The factor $|F^{\mathrm{n}}|/(|F^{\mathrm{n}}| + |F^{\mathrm{nl}}|)$ of Eq. (22) versus resolution using data from our model calculations

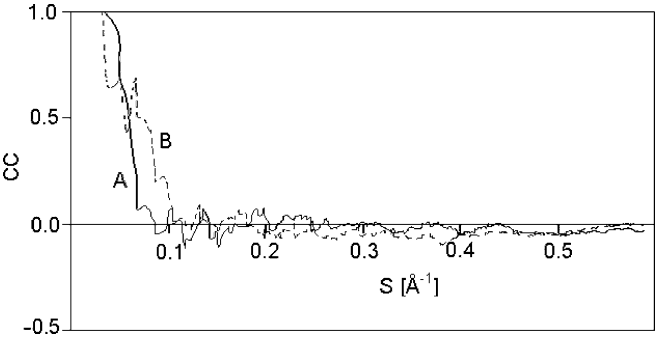


**Fig. 4** Curve *A*: the correlation coefficient between $\varphi^{\mathrm{l}}$ and $\varphi^{\mathrm{n}}$ (*full line*) versus resolution. Curve *B*: the correlation coefficient between two random variables in the range −180 to 180 (*dashed line*) versus size of the statistical samples mapped to resolution

fluctuates around 0.5 and that for resolution $S > 0.4$ the amplitudes of the fluctuations clearly become very small. This is the reason why the upper curve (squares) of Fig. 1 reaches asymptotically the value predicted by the DF method.

Finally, the third term in Eq. (22) contributes with noise because $\phi^{l}$ and $2\phi^{n}$ are not correlated. The manifestation of the absence of correlation between $\phi^{l}$ and $\phi^{n}$ in our model calculations is shown in Fig. 4 as a graph of their correlation coefficient versus resolution. In the same figure the correlation coefficient between two random variables in the range (−180, 180) is also presented. The similarity of these curves convinces us that $\phi^{l}$ and $2\phi^{n}$ are not correlated.

## References


Belrhali H, Nollert P, Royant A, Menzel C, Rosenbusch JP, Landau EM, Pebay-Peyroula E (1999) Protein, lipid and water organization in bacteriorhodopsin crystals: a molecular view of the purple membrane at 1.9 Å resolution. Struct Fold Des 7:909–917

Blundell TL, Johnson LN (1976) Protein crystallography. Academic Press, New York, p 407

Dencher NA, Büldt G, Heberle J, Höltje H-D, Höltje M (1992) In: Boundis T (ed) Proton transfer in hydrogen bonded systems. Plenum Press, New York, pp 171–185

Edholm O, Berger O, Jähnig F (1995) Structure and fluctuations of bacteriorhodopsin in the purple membrane: a molecular dynamics study. J Mol Biol 250:94–111

Ferrand M, Dianoux AJ, Petry W, Zaccai G (1993) Thermal motions and function of bacteriorhodopsin in purple membranes: effects of temperature and hydration studied by neutron scattering. Proc Natl Acad Sci USA 90:9668–9672

Hauss T, Büldt G, Heyn M, Dencher NA (1994) Light-induced isomerization causes an increase in the chromophore tilt in the M intermediate of bacteriorhodopsin: a neutron diffraction study. Proc Natl Acad Sci USA 91:11854–11858

Hauß T, Papadopoulos G, Verclas AW, Büldt G, Dencher NA (1997) Neutron diffraction on purple membranes: essential water molecules in the light-driven proton pump bacteriorhodopsin. Physica B 234–236:217–219

Henderson R, Baldwin JM, Downing KH, Lepault J, Zemlin F (1986) Structure of purple membrane from *Halobacterium halobium*: recording, measurement and evaluation of electron micrographs at 3.5 Å resolution. Ultramicroscopy 19:147–178

Killingbeck J, Cole GHA (1971) Mathematical techniques and physical applications. (Pure and applied physics series, vol 35) Academic Press, New York, p 252

Luecke H, Schobert B, H-T, Cartailler, J-P, Lanyi JK (1999) Structure of bacteriorhodopsin at 1.55 Å resolution. J Mol Biol 291:899–911

Papadopoulos G, Dencher NA, Zaccai G, Büldt G (1990) Water molecules and exchangeable hydrogen ions at the active centre of bacteriorhodopsin localized by neutron diffraction: elements of the proton pathway? J Mol Biol 214:15–19

Sass H-J, Büldt G, Gessenich R, Hehn D, Neff D, Schlesinger R, Berendzen J, Ormos P (2000) Structural alterations for proton translocation in the M state of wild-type bacteriorhodopsin. Nature 406:649–652

Subramanian S, Henderson R (2000) Molecular mechanism of vectorial proton translocation by bacteriorhodopsin. Nature 406:653–657

Thiedemann G, Heberle J, Dencher NA (1992) In: Rigaud JL (ed) Structures and functions of retinal proteins. Libby Eurotext, London, p 217

Zaccai G, Gilmore DJ (1979) Areas of hydration in the purple membrane of *Halobacterium halobium*: a neutron diffraction study. J Mol Biol 132:181–191